GA–A27405

EFFECT OF CHANGES IN SEPARATRIX MAGNETIC GEOMETRY ON DIVERTOR BEHAVIOR IN DIII-D

by

T.W. PETRIE, J.M. CANIK, C.J. LASNIER, A.W. LEONARD, M.A. MAHDAVI, J.G. WATKINS, M.E. FENSTERMACHER, J.R. FERRON, R.J. GROEBNER, D.N. HILL, A.W. HYATT, C.T. HOLCOMB, T.C. LUCE, R.A. MOYER, T.E. OSBORNE, AND P.C. STANGEBY

OCTOBER 2012

GENERAL ATOMICS

DISCLAIMER

GA–A27405

EFFECT OF CHANGES IN SEPARATRIX MAGNETIC GEOMETRY ON DIVERTOR BEHAVIOR IN DIII-D

by
T.W. PETRIE[1], J.M. CANIK[2], C.J. LASNIER[3], A.W. LEONARD[1], M.A. MAHDAVI[1], J.G. WATKINS[4], M.E. FENSTERMACHER[3], J.R. FERRON[1], R.J. GROEBNER[1], D.N. HILL[3], A.W. HYATT[1], C.T. HOLCOMB[3], T.C. LUCE[1], R.A. MOYER[5], T.E. OSBORNE[1], AND P.C. STANGEBY[6]

This is a preprint of a paper to be presented at the 24th IAEA Fusion Energy Conference, October 8–12, 2012, in San Diego, California

[1]General Atomics, P.O. Box 85608, San Diego, California, USA
[2]Oak Ridge National Laboratory, P.O. Box 2008, Oak Ridge, Tennessee, USA
[3]Lawrence Livermore National Laboratory, Livermore, California, USA
[4]Sandia National Laboratories, P.O. Box 5800, Albuquerque, New Mexico, USA
[5]University of California San Diego, La Jolla, California, USA
[6]University of Toronto Institute of Aerospace Studies, Toronto, Canada

Work supported by
the U.S. Department of Energy
under DE-FC02-04ER54698, DE-AC05-00OR22725, DE-AC52-07NA27344, DE-AC04-94AL85000, and DE-FG02-07ER54917

GENERAL ATOMICS PROJECT 30200
OCTOBER 2012

GENERAL ATOMICS

EFFECT OF CHANGES IN SEPARATRIX MAGNETIC GEOMETRY ON DIVERTOR BEHAVIOR IN DIII-D

T.W. Petrie[1], J.M. Canik[2], C.J. Lasnier[3], A.W. Leonard[1], M.A. Mahdavi[1], J.G. Watkins[4], M.E. Fenstermacher[3], J.R. Ferron[1], R.J. Groebner[1], D.N. Hill[3], A.W. Hyatt[1], C.T. Holcomb[3], T.C. Luce[1], R.A. Moyer[5], T.E. Osborne[1], and P.C. Stangeby[6]

[1]*General Atomics, P.O. Box 85608, San Diego, California 92186-5608, USA*
[2]*Oak Ridge National Laboratory, P.O. Box 2008, Oak Ridge, Tennessee 37831, USA*
[3]*Lawrence Livermore National Laboratory, Livermore, California 94550, USA*
[4]*Sandia National Laboratories, P.O. Box 5800, Albuquerque, New Mexico 87185, USA*
[5]*University of California-San Diego, La Jolla, California 92093-0417, USA*
[6]*University of Toronto Institute of Aerospace Studies, Toronto, Canada*

Abstract. We report results and interpretation of recent experiments on DIII-D designed to evaluate divertor geometries favorable for radiative heat dispersal. Two approaches studied involved lengthening the parallel connection in the scrape-off layer, $L_{||}$, and increasing the radius of the outer divertor separatrix strike point, R_{OSP}, with the goal of reducing target temperature, T_{TAR}, and increasing target density, n_{TAR}. Based on 1-D two-point modeling: $n_{TAR} \propto [R_{OSP}]^2 [L_{||}]^{6/7} [n_{SEP}]^3$ and $T_{TAR} \propto [R_{OSP}]^{-2} [L_{||}]]^{-4/7} [n_{SEP}]^{-2}$, where n_{SEP} is the midplane separatrix density. These scalings suggest that conditions conducive to a radiative divertor solution can be achieved at low n_{SEP} by increasing either R_{OSP} or $L_{||}$. Our data are consistent with the above $L_{||}$ scalings. On the other hand, the observed dependence of n_{TAR} and T_{TAR} on R_{OSP} displayed a more complex behavior, under certain conditions deviating from the above scalings. Our analysis indicates that deviations from the R_{OSP} scaling were due to the presence of convected heat flux, driven by escaping neutrals, in the more open configurations of the larger R_{OSP} cases.

1 Introduction

Future high-powered tokamaks will require a means of reducing heat load on the divertor targets. Prior investigations have shown that steady power load can be reduced with radiating divertor approaches [1–4] although projecting such approaches to future generation tokamaks is uncertain. Other approaches exploit divertor geometry, as, for example, with the Super-X [5] and Snowflake [6] concepts. In theory, power flow into the divertor can be dissipated and divertor temperature lowered by increasing the distance that heat from the main plasma entering the scrape-off layer (SOL) must traverse along a magnetic field line to the divertor target or by raising the radial isolation of the outer divertor target. These ideas are based on well-known physics in the SOL and can best be expressed at its simplest level using a one-dimensional Two-Point Model (TPM) [7]:

$$T_{TAR} \propto \left[P_{IN}\left(1-f_{RAD}\right)\right]^{10/7}\left(R_{TAR}n_{SEP}\right)^{-2}\left\{\left(f_R-1\right)/\left[L_{||}\ln\left(f_R\right)\right]\right\}^{4/7} \quad , \qquad (1)$$

and

$$n_{TAR} \propto \left[R_{TAR}\right]^2\left[n_{TAR}\right]^3\left[P_{IN}\left(1-f_{RAD}\right)\right]^{-8/7}\left\{\left[L_{||}\ln\left(f_R\right)\right]/\left(f_R-1\right)\right\}^{6/7} \quad , \qquad (2)$$

where R_{TAR} is the radial location of the outer divertor separatrix target, $L_{||}$ is the parallel connection length in the SOL between the midplane (or X-point) and the divertor target, n_{TAR} is the electron density at the outer divertor target, T_{TAR} is the electron temperature at the outer divertor target, n_{SEP} is the upstream electron density on the separatrix, P_{IN} is the power input, f_{RAD} is the fraction of radiated power, and f_R is the ratio R_{OSP}/R_{OMP}, where

R_{OMP} is the radial location of the separatrix at the outer midplane. These simple scalings suggest that conditions conducive to a radiative divertor solution can be achieved at lower n_{SEP} by increasing either R_{OSP} or $L_{||}$. We report results and interpretation of recent experiments on DIII-D designed to evaluate divertor geometries that might be favorable for radiative heat dispersal by testing how specific variations in R_{OSP} and $L_{||}$ affect n_{TAR}, T_{TAR}, and peak heat flux at the outer divertor target $Q_{\perp,0}$.

2 Experiment

The poloidal cross-sections of three of the plasma shapes used in this study are shown in Fig. 1. The maximum variation in radial placement of the outer divertor separatrix R_{OSP} for these lower single-null (SN) plasmas covers 1.20 m (black) to 1.71 m (green), as shown in Fig. 1. In this experiment, we distinguish between two regions of the divertor: *floor* and *shelf*, as shown. The *floor* region is much less open than the *shelf* region, which sits atop of the lower divertor baffle structure. The minimum and maximum *poloidal* extensions from the X-point to the outer divertor target for the plasmas in this experiment were 0.25 m (red) to 0.75 m (black), respectively, in Fig. 1. These poloidal distances correspond to parallel connection lengths $L_{||\text{-XPT}}$ of 17 m and 25 m, respectively. In all cases, the parallel path lengths in the SOL are referenced to the flux surface 0.15 cm radially outside the outer midplane separatrix.

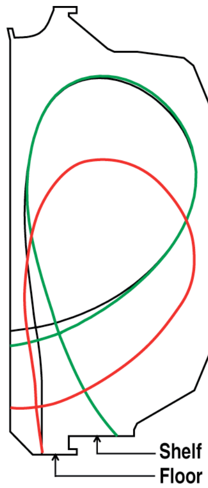

Fig. 1. The poloidal cross-sections of the MHD equilibria for three important cases discussed in this paper are shown. The floor and shelf regions of the lower divertor are indicated.

Upstream electron density and temperature were determined by Thomson scattering, while electron density and temperature downstream at the *outer* divertor target were based on Langmuir probe measurements. Heat flux across the lower divertor was deduced from infrared camera measurements. The ion $\boldsymbol{B} \times \nabla B$ drift was directed *toward* the X-point in all cases. There was no active particle pumping.

3 Results

3.1. Initial assessment of the dependence of n_{TAR}, T_{TAR}, and $Q_{\perp,0}$ on R_{OSP}

Two matched ELMing H-mode plasmas provided the data for comparison to Eqns (1) and (2), since their respective R_{OSP} represent the widest range possible in this experiment, i.e., 1.20 m (black) and 1.67 m (green) in Fig. 1. For either case, $n_e/n_G \approx 0.4$, H_{89P}≈1.6, and $f_{RAD} \approx 0.4$. Edge and divertor properties aresummarized in Table 1. The dependence of n_{TAR} and T_{TAR} did not follow TPM predictions of Eqns (1) and (2), i.e., n_{TAR} should *increase* by ≈20% and T_{TAR} should *decrease* by ≈26% between the R_{OSP} = 1.20 m and 1.67 m. From experiment, however, n_{TAR} decreased by ≈51% and increased by ≈33% (Table 1). In addition, the peak heat flux at the outer divertor target $Q_{\perp,0}$ was ≈25% higher for the R_{OSP} = 1.67 m case.

3.2. R_{OSP} scans in L-mode and H-mode

Results from a radial sweep of the outer strike point (OSP) across both *floor* and *shelf*, shown in Fig. 2, demonstrates the n_{TAR} and T_{TAR} behaviors *between* these R_{OSP} endpoints. The endpoints of this sweep in L-mode were R_{OSP} = 1.20 m and 1.60 m. Figure 2 indicates that the n_{TAR} and T_{TAR} behaviors qualitatively track the predictions of the Two-Point Model across the floor and the shelf, *individually*. Both n_{TAR} and T_{TAR} have much stronger dependences on R_{OSP} along the floor than the "expected" quadratic dependence from the TPM. However, n_{TAR} and T_{TAR} on the shelf have a weaker dependence on R_{OSP} compared with the *floor* result and are more in-line with TPM. Figure 2 suggests that there may a discontinuity in both n_{TAR} and T_{TAR} across the floor-shelf boundary. Note that when one only considers the n_{TAR} and T_{TAR} values at the endpoints, the results in Sec. 3.1 and Table 1 are qualitatively recovered.

In order to examine H-mode behavior, a modest radial sweep of the OSP across the *floor* was used to assess changes to the divertor plasma due to the proximity of the baffle facing at R = 1.37 m. Because any shape changes in the main plasma were minimized by the limited range of the radial sweep (i.e., $R_{OSP} \approx$ 1.21–1.30 m), ELMing H-mode core properties remained fairly constant over the sweep, e.g., H_{89P} = 1.9–2.0 and $n_{SEP} \approx 0.85 \times 10^{19}$ m^{-3}. Like the L-mode case above, the response of n_{TAR} and T_{TAR} to changes in R_{OSP} was considerably stronger than expected from the TPM (Fig. 3). Density and temperature data from two H-mode shots having comparable core plasma characteristics but with their OSP on the shelf are also shown. As in the L-mode case with OSP on the shelf, n_{TAR} increased with R_{OSP} and T_{TAR} decreased with R_{OSP}, although still with a somewhat higher dependence on R_{OSP} than predicted by TPM. As in the L-mode case, there

Table 1. Large R_{OSP} vs. low R_{OSP}

	Low R_{OSP}	High R_{OSP}
Shot	146010	145878
R_{OSP} (m)	1.20	1.67
$L_{\parallel-XPT}$ (m)	25	20
X-point height (m)	0.75	0.75
$n_{SEP}\left(10^{19}\ \mathrm{m}^{-3}\right)$	0.91	0.92
T_{SEP} (eV)	91	71
$n_{TAR}\left(10^{19}\ \mathrm{m}^{-3}\right)$	3.4	1.7
T_{TAR} (eV)	18.0	24.0
$Q_{\perp,0}$ (MW/m^2)	1.2	1.5

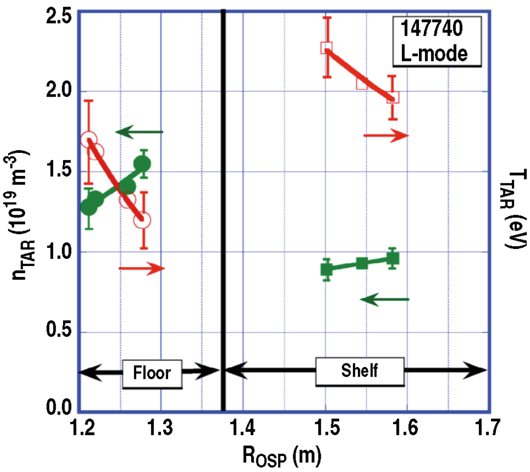

Fig. 2. n_{TAR} (closed) and T_{TAR} (open) are shown as a function of R_{TAR}: I_P = 0.8 MA, q_{95} = 3.8, P_{IN} = 1.2 MW, $P_{RAD}/P_{IN} \approx 0.35$, and $n_e/n_G \approx 0.2$.

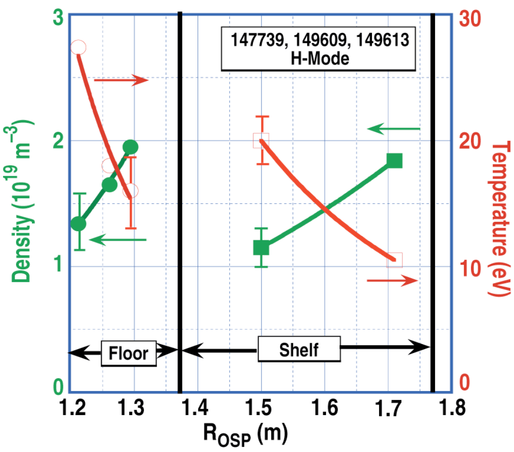

Fig. 3. n_{TAR} (closed) and T_{TAR} (open) are shown as a function of R_{OSP}: I_P = 0.8 MA, q_{95} = 3.9–4.3, P_{IN} = 4.9 MW, H_{89P} = 1.6–1.9, $P_{RAD}/P_{IN} \cong 0.35$–0.45, and $n_e/n_G \cong$ 0.35. A vertical barrier defining the outer boundary of the shelf is shown.

is no apparent monotonic trend for either n_{TAR} or T_{TAR} across both floor and shelf. These results may be explained by the degree by which neutrals are trapped by the baffle structure, as we discuss later in this paper.

As R_{OSP} on the floor approached the baffle structure, $Q_{\perp,0}$ decreased. However, $Q_{\perp,0}$ was considerably greater when R_{OSP} was located on the shelf (Fig. 4) and its dependence on R_{OSP} was not monotonic [Fig. 5(a)]. This result can be partially explained by noting that the poloidal flux expansion (f_{EXP}) and the angle between the poloidal separatrix flux surface and the divertor target (θ_T) both increase with R_{OSP}. From geometry alone one expects that $Q_{\perp,0} \propto \sin\theta_T$ / [R_{OSP} x f_{EXP}]. Based on the θ_T and f_{EXP} values (listed in the caption to Fig. 5), one expects that $Q_{\perp,0}$ to behave with R_{OSP} as represented by the "open" symbols shown in Fig. 5(a); note that $Q_{\perp,0}$ has been normalized to the $Q_{\perp,0}$ value at R_{OSP} = 1.40 m case. The difference in the $Q_{\perp,0}$ based on geometrical considerations and the measured $Q_{\perp,0}$ increases with R_{OSP}. Interestingly, the full-width at half maximum (FWHM) of the measured heat flux profiles on the shelf is approximately constant (≈2 cm) with changes in R_{OSP}. This result would not be expected if geometry were the only consideration, since the range in f_{EXP} on the shelf is 1.3–3.2. These measured heat flux profiles on the shelf can be mapped back to the outer midplane along SOL field lines. The resulting parallel heat flux profile referenced to the outer midplane ($q_{||}$) is useful for factoring out geometric effects of heat flowing to the divertor target. The peak in parallel heat flux at the midplane ($q_{||,0}$) is found to fall off rapidly with increasing R_{OSP} [Fig. 5(b)], while the FWHM of the $q_{||}$ profile strongly increased with R_{OSP} (Fig. 5(c)). Our explanation for this behavior will be discussed in Sec. 4.

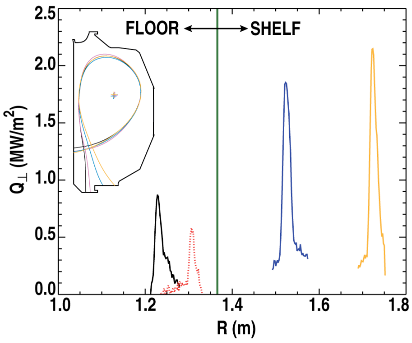

Fig. 4. The heat flux profiles [$Q_\perp$] are plotted as a function of divertor radial location R for the cases shown in Fig. 3.

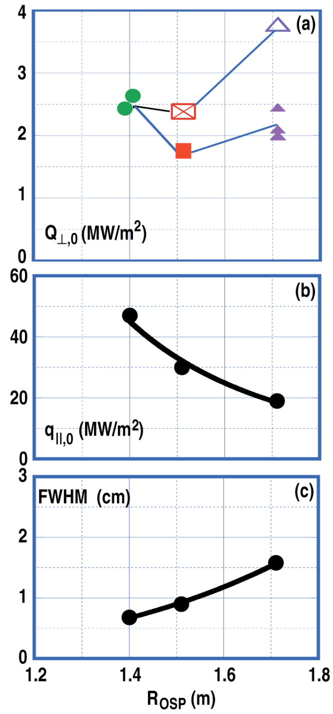

Fig. 5. (a) Measured peak heat flux on the shelf (solid) and peak heat flux based on geometry (open); f_{EXP} = 3.2, 2.5, 1.3 and θ_T = 70°, 50°, 45° for R_{OSP} = 1.40 m, 1.51 m, 1.71 m cases, respectively, (b) $q_{||,0}$, (c) FWHM of the $q_{||}$ profile.

3.3. Variation of heat flux under higher density, radiating divertor conditions

The data presented in Sec. 3.2 suggests that locating the OSP on the floor adjacent to the baffle structure produces a significantly different divertor heat flux than placing the OSP a few centimeters outboard of that location on the shelf. In this section we examine this idea more closely by comparing two R_{OSP} cases, i.e., 1.30 m (floor) and 1.40 m (shelf). We will refer to the former as the "closed" divertor configuration and the latter as the "open" divertor configuration. Figure 6(a) shows that the time-averaged peak heat flux (which include ELMs) $\langle Q_{\perp,0} \rangle$ in the closed configuration was ~20% lower than in the open configuration at the lowest density; this 20% difference was also observed when comparing respective $q_{\|,0}$ values, where the FWHM of the 1.30 m case was ~20% higher. This difference increased as core density was raised. The OSP in the closed configuration detached *between* ELMs well before evidence of detachment occurred in the open configuration [Fig. 6(a)]. This difference in $\langle Q_{\perp,0} \rangle$ between open and closed divertor cases primarily occurred between ELM events [Fig. 6(b)] and not during ELMs [Fig. 6(c)]. Note that whether the divertor was open or closed at any given density considered here produced little difference on $Q_{\perp,0}$ during ELMing events. Even though the peak heat flux was significantly lower in the closed configuration at any given density, whether the divertor was "open" or "closed" made no difference in the normalized energy confinement, pedestal density, and pedestal temperature when compared at a common density. Isolating the divertor target from the core plasma ($L_{\|\text{-XPT}}$ = 25 m) may have been helpful in this regard. The closed configuration extended the operating range to lower core density while still maintaining a lower value of heat flux. For example, if the allowable upper limit for $\langle Q_{\perp,0} \rangle$ were set to 2 MW/m^2, then Fig. 6(a) shows that it is possible to operate at a lower line-averaged density in the closed divertor case than with the open divertor case, i.e., ≈3.4x10^{19} m^{-3} vs ≈4.0x10^{19} m^{-3}.

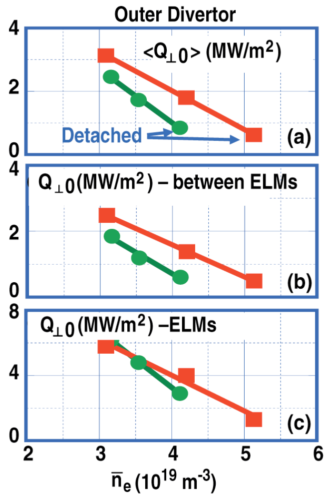

Fig. 6. (a) $\langle Q_{\perp,0} \rangle$, (b) "between-ELM" $Q_{\perp,0}$, and (c) $Q_{\perp,0}$ during ELMs are shown vs n_e for the "open"[(R_{OSP} = 1.40 m (red)] and "closed" [R_{OSP} = 1.30 m (green)] configurations.

3.4. Variation of n_{TAR}, T_{TAR}, and $Q_{\perp,0}$ with $L_{\|\text{-XPT}}$

Equations (1) and (2) predict that lengthening the outer divertor leg increases n_{TAR} and decreases T_{TAR}. To test this, we compared two H-mode plasmas having significantly different $L_{\|\text{-XPT}}$ but virtually the same R_{OSP}. Their shapes are shown as the black (high X-point) and red (low X-point) curves in Fig. 1. Langmuir probe measurements indicate that the case with larger $L_{\|\text{-XPT}}$ (=25 m) resulted in higher n_{TAR} and lower T_{TAR} (Table 2). This is in qualitative agreement with TPM predictions. Equations (1) and (2) can be combined with data from the lower $L_{\|\text{-XPT}}$ (=17 m) case (Table 2) to predict n_{TAR} and T_{TAR} for the $L_{\|\text{-XPT}}$ (= 25 m) case. The two-point model predicts for the longer parallel connection length case: $n_{TAR} \approx 4.6\text{x}10^{19}$ m^{-3} and $T_{TAR} \approx 17$ eV. These are in quantitative agreement with the actual measurements for the higher X-point case (Table 2).

Although f_{EXP} was lower for the $L_{\parallel\text{-XPT}}$ = 25 m case, i.e., ≈3.2 versus ≈5.6 for the $L_{\parallel\text{-XPT}}$ = 17 m case, the peak heat flux $Q_{\perp,0}$ was greater in the latter, as shown in Fig. 7. The FWHM of the deposited heat flux profiles in both cases was comparable, i.e., ≈ 3.5 cm; not surprisingly, $q_{\parallel,0}$ for the $L_{\parallel\text{-XPT}}$ = 25 m case was roughly half that of the 17 m case and its FWHM of $q_{\parallel}$ was roughly double. This result is consistent with the idea of competing parallel and perpendicular transport on field lines in the SOL, which we discuss in the following section.

Table 2. High X-point vs. low X-point

	High X-point	Low X-point
X-point height (m)	0.75	0.25
$L_{\parallel\text{-XPT}}$ (m)	25	17
R_{OSP} (m) (m)	1.20	1.21
$n_{SEP}\left(10^{19}\ \mathrm{m}^{-3}\right)$	1.03	1.01
T_{SEP} (eV)	74	84
$n_{TAR}\left(10^{19}\ \mathrm{m}^{-3}\right)$	4.4	3.2
T_{TAR} (eV)	17.0	21.5

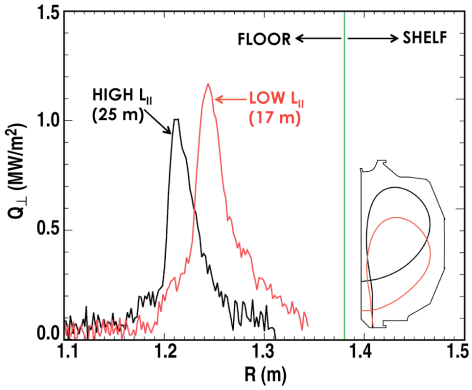

Fig. 7. $Q_{\perp}$ profiles are plotted vs radial location for the low- and high X-point cases: I_P = 0.8 MA, P_{IN} = 5 MW, P_{RAD}/P_{IN} ≈ 0.45, n_{SEP} ≈ 1.0x10^{19} m^{-3}, T_{SEP} ≈ 80 eV, n_e/n_G ≈ 0.35, H_{89P} ≈ 1.4–1.8.

4 Discussion

Modeling of the edge and divertor plasmas was done using the SOLPS suite of codes [8], which provide a 2-D model to couple plasma and neutral transport. The plasma transport was calculated using the fluid code B2 [9] and the neutral transport was calculated using the Monte-Carlo code EIRENE [10]. Classical drifts were not included. SOLPS was used in an interpretive sense, with the primary constraint being the measured midplane density and temperature profiles, which were matched in the simulation by adjusting the specified radially varying, poloidally constant transport coefficients [11]. No anomalous convection was included, so these represent "effective" cross-field diffusivities. The measured divertor heat flux effectively constrained the position of the midplane profiles relative to the separatrix. With the midplane data matched to the measured profiles, the simulated divertor density and temperature profiles were then compared to the measured values.

SOLPS calculations for the two R_{OSP} cases discussed in Sec. 3.1 show that with $Q_{\perp,0}$ constrained by measurement n_{TAR} and T_{TAR} are in qualitative agreement with experiment. SOLPS modeling indicates that n_{TAR} is higher and both T_{TAR} and $Q_{\perp,0}$ are lower for the low R_{OSP} = 1.20 m case. Both T_{TAR} and $Q_{\perp,0}$ are in reasonable quantitative agreement (~25%) with the data. The experimental n_{TAR} is well within a factor of two in either R_{OSP} case, and is qualitatively in agreement. SOLPS/EIRENE modeling indicate more neutrals escape the outer divertor target in the more open configuration R_{OSP} = 1.67 m case. A fraction of these neutrals return to the SOL plasma upstream of the target, are ionized, and flow back to the target, thereby increasing the convective component of the parallel power flow to the divertor target more than would occur in the more closed configuration (R_{OSP} = 1.20 m case). Increasing the convective component of the power flow can be expected to increase T_{TAR} and reduce n_{TAR} [12]. For a location slightly upstream of the divertor target, SOLPS modeling indicates that, for the R_{OSP} = 1.67 m case, convection carries virtually the entire heat flux outside the radial location of the FWHM of the $Q_{\perp}$ profile, while for the R_{OSP} =

1.20 m case at FWHM of the $Q_\perp$ profile, conduction still plays a substantial role (~30%). It is worth noting that the role of neutral trapping has been confirmed by performing SOLPS simulations with the *baffle structure removed* so that neutral trapping in both cases are similar; the result was to reverse the trends of $n_{\rm TAR}$ and $T_{\rm TAR}$ with $R_{\rm OSP}$ discussed above.

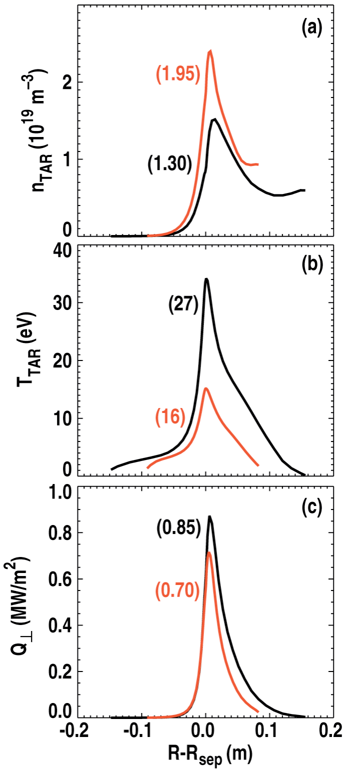

Fig. 8. SOLPS modeling for two H-mode cases in Sec. 3.2, where R_{OSP} = 1.21 m (black) and R_{OSP} = 1.30 m (red). (a) n_{TAR}, (b) T_{TAR}, and (c) $Q_\perp$ are shown vs divertor separatrix location R_{SEP}. The experimental peak values are quoted in parenthesis next to the SOLPS predictions.

The neutrals trapping effect is particularly evident in the radial sweep in $R_{\rm OSP}$ (Sec. 3.2). SOLPS modeling showed that the baffle structure had an important role in determining divertor properties. For the endpoints of this sweep, i.e., $R_{\rm OSP}$ = 1.21 m and 1.30 m with $Q_{\perp,0}$ constrained by measurement, SOLPS indicates that $T_{\rm TAR}$ was reduced as $R_{\rm OSP}$ was moved from 1.21 m to 1.30 m. This result was in reasonable agreement with experiment, both qualitatively and quantitatively (Fig. 8). In addition, $n_{\rm TAR}$ increased with $R_{\rm OSP}$, again in agreement with experiment. Modeling shows that with greater proximity of the OSP to the baffle structure enhanced neutral trapping. Increased neutral trapping raised recycling, resulting in increased $n_{\rm TAR}$ and lowered $T_{\rm TAR}$. This is consistent with observation. As $R_{\rm TAR}$ was moved toward the baffle structure, neutral pressure measured in the lower divertor pumping plenum increased by a factor of 3–4, and D_α-emissivity increased by a factor of ≈2. These observations indicate the increased presence of neutrals near the outer divertor target. Furthermore, the higher $n_{\rm TAR}$ and lower $T_{\rm TAR}$ conditions in the $R_{\rm OSP}$ = 1.30 m case resulted in an increase in radiated power along the outer divertor leg (≈30%) and was clearly helpful in reducing $Q_{\perp,0}$. To a lesser degree, this behavior was observed on the more open shelf top, where the barrier on the high-R side of the shelf can still trap neutrals in the SOL of the $R_{\rm OSP}$ = 1.71 m case more effectively than in the $R_{\rm OSP}$ = 1.51 m case.

The above discussion covering the large vs. small $R_{\rm OSP}$ experiment and the $R_{\rm OSP}$ sweep experiment both illustrate the role of neutrals trapping and its contribution to upstream convection along the outer divertor leg. This applies to the results from the "closed" (with effective neutrals trapping) vs "open" (with considerably less effective neutrals trapping) divertor experiment (Sec. 3.3). The result is that the peak heat in the "closed" case is lower than that of the "open" case at upstream similar density and detachment is possible in the former at lower density.

Changing the parallel connection length $L_{||\text{-XPT}}$ in the SOL resulted in behaviors in $n_{\rm TAR}$ and $T_{\rm TAR}$ largely in agreement with the TPM. More generally, cross-field diffusion can also affect these results, if $L_{||\text{-XPT}}$ differs significantly, as in Sec. 3.4. One formulation, which has attempted to factor in cross-field transport [12], concludes a slightly stronger contribution from $L_{||\text{-XPT}}$ to $n_{\rm TAR}$ and $T_{\rm TAR}$ than predicted by Eqns (1) and (2), although for the cases discussed in this paper this effect produced little difference between these 1D and 2D predictions. However, $Q_{\perp,0}$ was *lower* for the case with lower f_{EXP}, i.e., the high X-point case; this would be unexpected, based on geometrical considerations only. In addition, the FWHM of $Q_{\perp}$ in both cases was almost the same. Increasing the connection length affected $Q_{\perp,0}$ and its profile width as much as the purely geometric effect of increasing f_{EXP}. SOLPS results indicate that increased cross-field transport effects were clearly involved, so that, as $L_{||}$ increased, the width of the heat flux at the target also increased. The presence of such cross-field energy transport should be particularly evident in cases when f_{EXP} is small and connection length is relatively long. This is the case of R_{OSP} = 1.71 m, f_{EXP} = 1.3, and $L_{||\text{-XPT}}$ = 21 m in the R_{OSP} scan in Fig. 5. In the cases where R_{OSP} = 1.51 m and 1.40 m, f_{EXP} is much higher, so that energy transport across field lines, which depend on spatial gradient, would be more masked.

In summary, we find that experiment and 2-D modeling show overall improved divertor conditions with larger SOL connection length and R_{OSP}.

This work was supported by the U.S. Department of Energy under DE-FC02-04ER54698, DE-AC05-00OR22725, DE-AC52-07NA27344, DE-AC04-94AL85000, DE-FG02-07ER54917, and DE-FG02-05ER54809.

References

[1] GOETZ, J.A., et al., J. Nucl. Mater. **266–269** (1999) 359.
[2] RAPP, J., et al., Nucl. Fusion **44** (2004) 312.
[3] KALLENBACH, A., et al., J. Nucl. Mater. **337–339** (2005) 732.
[4] PETRIE, T.W., et al., J. Nucl. Mater. **363–365** (2007) 416.
[5] KOTSCHENREUTHER, M., Phys. Plasmas **14** (2007) 072502.
[6] RYUTOV, D., Phys. Plasmas **14** (2007) 06452.
[7] STANGEBY, P.C., (private communication).
[8] SCHNEIDER, R., et al., Contrib. Plasma Phys. **46** (2006) 3.
[9] BRAAMS, B.J., Contrib. Plasma Phys. **36** (1996) 276.
[10] REITER, D., et al., Fusion Sci. Tech. **47** (2005) 172 and www.eirene.de.
[11] CANIK, J.M., et al., J. Nucl. Mater. **415** (2011) S409.
[12] STANGEBY, P.C., The Plasma Boundary of Magnetic Fusion Devices, IOP Publishing (2002) Chapter 5.